

Supporting Information

A family of CuI-based 1D polymers showing colorful short-lived TADF and phosphorescence induced by photo- and X-ray irradiation

Alexander V. Artem'ev,^{a*} Evgeniya P. Doronina,^b Mariana I. Rakhmanova,^a Xiuze Hei,^c Dmitri V. Stass,^{d,e} Ol'ga A. Tarasova,^b Irina Yu. Bagryanskaya,^f Denis G. Samsonenko,^a Alexander S. Novikov,^{j,h} Nina A. Nedolya,^b and Jing Li^{c*}

^a *Nikolaev Institute of Inorganic Chemistry, SB RAS, 3 Acad. Lavrentiev Ave., Novosibirsk, 630090, Russia*

^b *A. E. Favorsky Irkutsk Institute of Chemistry, SB RAS, 1 Favorsky Str., Irkutsk, 664033 Russia*

^c *Department of Chemistry and Chemical Biology, Rutgers University, Piscataway, New Jersey 08854, United States*

^d *V. V. Voevodsky Institute of Chemical Kinetics and Combustion, SB RAS, 3 Institutskaya Str., Novosibirsk, 630090, Russia*

^e *Department of Physics, Novosibirsk State University, 2 Pirogova St., Novosibirsk, 630090, Russia*

^f *N. N. Vorozhtsov Novosibirsk Institute of Organic Chemistry, SB RAS, 9 Acad. Lavrentiev Ave., Novosibirsk, 630090, Russia*

^j *Saint Petersburg State University, 7/9 Universitetskaya Nab., Saint Petersburg, 199034, Russia*

^h *Peoples' Friendship University of Russia (RUDN University), 6 Miklukho-Maklaya St, Moscow, 117198, Russia*

*Authors for correspondence: chemisufarm@yandex.ru (Alexander V. Artem'ev), jingli@rutgers.edu (Jing Li)

Table of contents

S2	§1. General details and instrumentations
S2–6	§2. Synthesis and characterization data
S6–12	§3. Single crystal X-Ray crystallography
S12–13	§4. Powder X-ray diffraction patterns
S13–14	§5. TGA&DTG curves
S14	§6. FT-IR spectra
S14–15	§7.1. Electronic structure calculations
S15–17	§7.2. QTAIM and ELF calculations
S17–19	§8. Photophysical data
S19–22	§9. X-Ray radioluminescence
S23–24	§10. References

§1. General details and instrumentations

All reactions were carried out at ambient temperature on air. 2-Methylthiopyridine (>98.0%, TCI) was used as commercial product, and other employed 2-methylthiopyridines were prepared as previously described.^{1,2} CuI ($\geq 99.0\%$, Aldrich) and MeCN (HPLC grade, Cryochrom) were used without further purification.

The CHN microanalyses were performed on a MICRO cube analyzer.

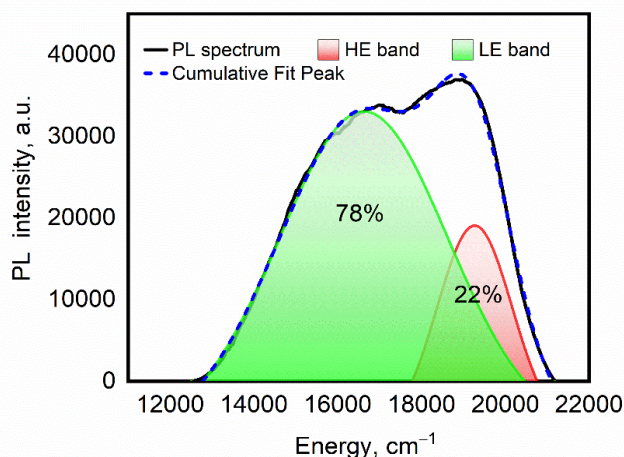
Powder X-ray diffraction analyses (PXRD) were made on a Shimadzu XRD-7000 diffractometer (Cu-K α radiation, Ni – filter, 3–35° 2 θ range, 0.03° 2 θ step, 5s per point).

Thermogravimetric analyses (TGA&DTG&c-DTA) were carried out in a closed Al₂O₃ pan under argon flow at 10 °C/min⁻¹ heating rate using a NETZSCH STA 449 F1 Jupiter STA instrument.

FT-IR spectra were recorded on a Bruker Vertex 80 spectrometer in KBr pellets at ambient temperature.

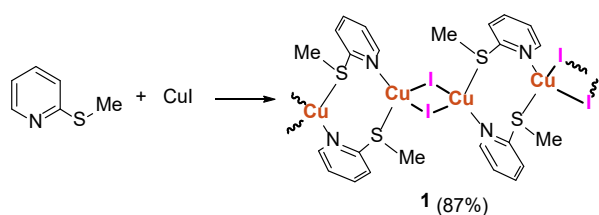
Diffuse reflectance spectra were registered on a Shimadzu UV-3101 spectrophotometer. Samples were prepared by a grinding of a complex (10 mol%) with BaSO₄. The reflectance data were converted into absorption spectra applying a Kubelka–Munk function.

Steady-state excitation and emission spectra were recorded on a Fluorolog 3 spectrometer (Horiba Jobin Yvon) equipped with a cooled PC177CE-010 photon detection module and an R2658 photomultiplier. The emission decays were recorded on the same instrument. The absolute PLQYs were determined at 298 K using a Fluorolog 3 Quanta-phi integrating sphere. Temperature-dependent excitation and emission spectra as well as emission decays were recorded using an Optistat DN optical cryostat (Oxford Instruments) integrated with above spectrometer. To evaluate k_r and k_{nr} values for HE and LE of CP **3**, its PL spectrum was deconvoluted into two Gaussian functions (see figure below), and their integrated intensities were used for evaluation of the quantum yields for each band.



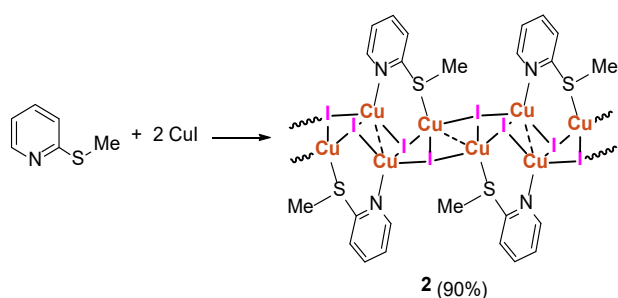
§2. Synthesis and characterization data

CP 1



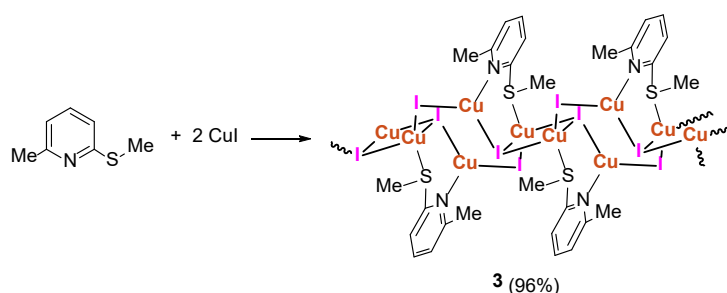
To a stirred solution of 2-(methylsulfanyl)pyridine (71 mg, 0.57 mmol) in MeCN (6 mL), CuI (108 mg, 0.57 mmol) was added. The suspension was stirred until dissolution of CuI, and the resulting solution was then filtered and slowly evaporated on air for overnight. The precipitated colorless crystals of **1** were collected and dried on air. Yield: 156 mg (87%). Anal. Calcd. for C₆H₇CuINS (315.64): C, 22.8; H, 2.2; N, 4.4. Found: C, 22.7; H, 2.1; N, 4.5. FT-IR (KBr, cm⁻¹): ν = 411 (w), 428 (w), 486 (m), 635 (w), 708 (m), 754 (s), 764 (s), 870 (w), 968 (s), 986 (m), 1005 (m), 1049 (m), 1092 (m), 1130 (s), 1159 (s), 1233 (m), 1275 (m), 1422 (vs), 1427 (m), 1449 (s), 1557 (s), 1578 (s), 1595 (w), 2916 (w), 2988 (w), 3053 (w), 3063 (w), 3075 (w), 3092 (w).

CP 2



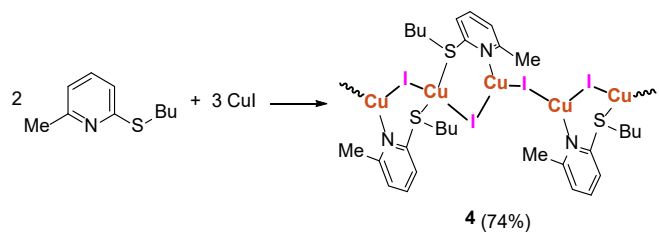
The mixture of CuI (213 mg, 1.12 mmol) and 2-(methylsulfanyl)pyridine (70 mg, 0.56 mmol) in MeCN (7 mL) was stirred for overnight. The precipitated white microcrystalline powder of **2** was centrifuged and dried in vacuum. Yield: 255 mg (90%). Anal. Calcd. for C₆H₇Cu₂I₂NS (506.09): C, 14.2; H, 1.4; N, 2.8. Found: C, 14.1; H, 1.6; N, 2.8. FT-IR (KBr, cm⁻¹): ν = 378 (w), 386 (w), 411 (m), 428 (w), 484 (m), 637 (m), 698 (m), 725 (m), 731 (m), 758 (vs), 876 (m), 961 (m), 970 (m), 1005 (m), 1055 (m), 1096 (m), 1130 (m), 1159 (m), 1233 (m), 1283 (m), 1317 (m), 1422 (vs), 1456 (s), 1479 (w), 1557 (m), 1580 (m), 2905 (w), 2914 (w), 2988 (w), 3001 (w), 3059 (w).

CP 3



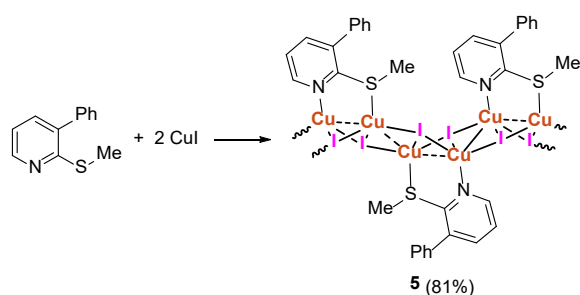
The mixture of CuI (200 mg, 1.05 mmol) and 2-methyl-6-(methylsulfanyl)pyridine (110 mg, 0.79 mmol) in MeCN (3 mL) was stirred for overnight. The precipitated colorless microcrystalline powder of **3** was filtered and dried in vacuum. Yield: 262 mg (96%). Anal. Calcd. for C₇H₉Cu₂I₂NS (520.12): C, 16.2; H, 1.7; N, 2.7. Found: C, 16.1; H, 1.8; N, 2.5. FT-IR (KBr, cm⁻¹): ν = 382 (w), 426 (w), 563 (w), 681 (m), 725 (m), 777 (s), 870 (m), 961 (s), 997 (m), 1013 (m), 1038 (m), 1088 (m), 1150 (m), 1173 (s), 1240 (m), 1308 (m), 1387 (m), 1418 (s), 1449 (vs), 1558 (s), 1584 (s), 2853 (w), 2913 (w), 2990 (w), 3044 (w).

CP 4



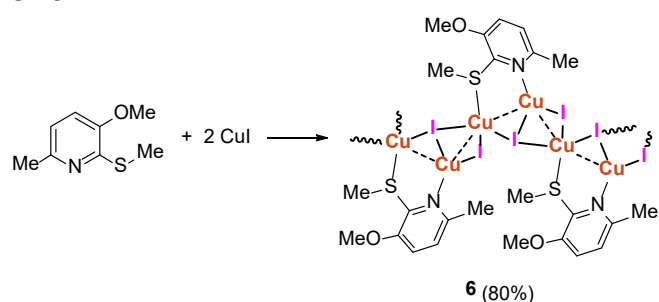
A mixture of 2-(butylsulfanyl)-6-methylpyridine (82 mg, 0.45 mmol) and CuI (86 mg, 0.45 mmol) in MeCN (6 mL) was stirred until dissolution of CuI, and the resulting solution was then filtered and slowly evaporated on air for overnight. The precipitated colorless crystals of **4** were collected and dried on air. Yield: 104 mg (74%). Anal. Calcd. for $C_{20}H_{30}Cu_3I_3N_2S_2$ (933.95): C, 25.7; H, 3.2; N, 3.0. Found: C, 25.8; H, 3.4; N, 2.9. FT-IR (KBr, cm^{-1}): $\nu = 378$ (vw), 393 (w), 418 (vw), 442 (w), 463 (vw), 561 (w), 685 (w), 731 (m), 741 (w), 779 (vs), 797 (w), 864 (w), 893 (w), 922 (w), 991 (w), 1013 (w), 1030 (vw), 1061 (vw), 1099 (w), 1148 (w), 1178 (s), 1223 (w), 1240 (w), 1306 (w), 1373 (m), 1427 (s), 1450 (vs), 1464 (m), 1545 (m), 1558 (m), 1587 (m), 1668 (w), 2853 (m), 2868 (m), 2920 (m), 2926 (m), 2955 (s), 3057 (w).

CP 5



The mixture of CuI (280 mg, 1.56 mmol), 2-(methylsulfanyl)-3-phenylpyridine (296 mg, 1.40 mmol) and several drops of MeCN was ground with a pestle for several minutes. The off-white solid was sequentially treated with aqueous solution of KI (5 mL, 10 M) and water to remove unreacted CuI. The resulting powder of **5** was further dried in vacuum. Yield: 413 mg (91%). Anal. Calcd. for $C_{12}H_{11}Cu_2I_2NS$ (582.19): C, 24.8; H, 1.9; N, 2.4. Found: C, 24.5; H, 1.8; N, 2.5. FT-IR (KBr, cm^{-1}): $\nu = 409$ (w), 446 (w), 490 (w), 542 (w), 565 (w), 687 (m), 706 (vs), 746 (m), 764 (vs), 804 (m), 856 (w), 922 (w), 972 (m), 1009 (m), 1065 (m), 1072 (m), 1109 (m), 1215 (m), 1312 (m), 1391 (vs), 1439 (s), 1495 (w), 1562 (m), 1572 (w), 2853 (w), 2924 (w), 3009 (w), 3046 (w).

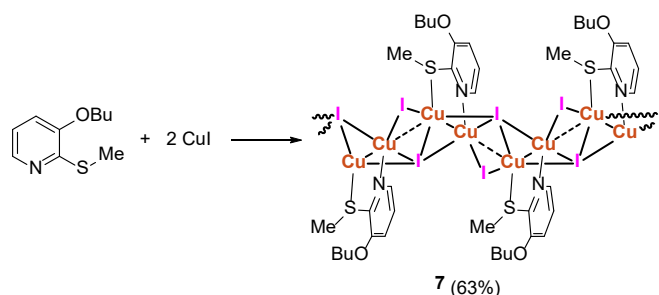
CP 6



The mixture of CuI (263 mg, 1.38 mmol), 3-methoxy-6-methyl-2-(methylsulfanyl)pyridine (141 mg, 0.83 mmol) and several drops of MeCN was ground with a pestle for several minutes. The off-white solid was sequentially treated with aqueous solution of KI (5 mL, 10 M) and water to remove unreacted CuI. The resulting powder of **6** was further dried in vacuum. Off-white powder. Yield: 304 mg (80%). Anal. Calcd. for $C_8H_{11}Cu_2I_2NOS$ (550.14): C, 17.5; H, 2.0; N, 2.5. Found: C, 17.4; H, 2.2; N, 2.2. FT-IR (KBr, cm^{-1}): $\nu = 426$ (vw), 583 (w), 669 (vw), 760 (w), 800 (w), 829 (m), 978 (w), 1018 (m), 1103 (m), 1246 (m), 1256 (m), 1275 (vs),

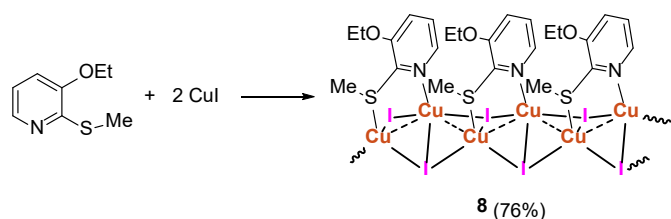
1327 (w), 1379 (w), 1431 (s), 1452 (m), 1466 (s), 1558 (m), 1742 (w), 2833 (w), 2874 (w), 2936 (w), 2963 (w), 3001 (w), 3069 (w).

CP 7



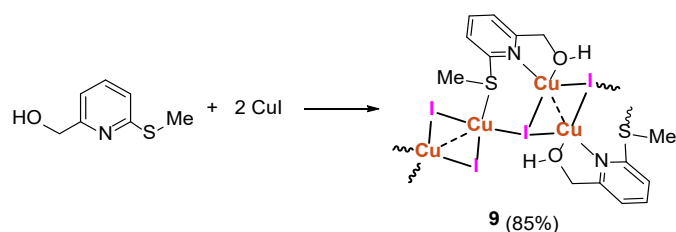
A mixture of 3-butoxy-2-(methylsulfanyl)pyridine (78 mg, 0.39 mmol) and CuI (75 mg, 0.39 mmol) in MeCN (3 mL) was stirred until dissolution of CuI, and the resulting solution was then filtered and slowly evaporated on air for overnight. The formed yellowish crystals of **7** were collected and dried on air. Yield: 72 mg (63%). Anal. Calcd. for $C_{10}H_{15}Cu_2I_2NOS$ (578.20): C, 20.8; H, 2.6; N, 2.4. Found: C, 20.8; H, 2.7; N, 2.2. FT-IR (KBr, cm^{-1}): $\nu = 532$ (w), 565 (m), 610 (m), 689 (m), 706 (m), 731 (m), 758 (m), 799 (s), 818 (w), 839 (m), 881 (m), 914 (m), 962 (s), 972 (s), 1003 (m), 1063 (m), 1097 (s), 1121 (m), 1144 (m), 1206 (m), 1219 (s), 1248 (s), 1283 (vs), 1395 (m), 1414 (m), 1443 (s), 1562 (s), 2858 (m), 2930 (m), 2953 (m), 3067 (w).

CP 8



A mixture of 3-ethoxy-2-(methylsulfanyl)pyridine (76 mg, 0.45 mmol) and CuI (85 mg, 0.45 mmol) in MeCN (3 mL) was stirred until dissolution of CuI, and the resulting solution was then filtered and slowly evaporated on air for overnight. The formed yellowish microcrystals of **8** were collected and dried on air. Yield: 93 mg (76%). Anal. Calcd. for $C_8H_{11}Cu_2I_2NOS$ (550.14): C, 17.5; H, 2.0; N, 2.5. Found: C, 17.7; H, 1.9; N, 2.4. FT-IR (KBr, cm^{-1}): $\nu = 503$ (w), 546 (w), 563 (m), 613 (m), 708 (m), 739 (m), 797 (s), 820 (m), 928 (m), 957 (m), 970 (m), 1034 (s), 1096 (m), 1111 (s), 1134 (s), 1209 (m), 1219 (m), 1254 (m), 1287 (vs), 1302 (m), 1389 (s), 1422 (m), 1443 (s), 1476 (w), 1560 (s), 1578 (w), 2860 (w), 2897 (w), 2922 (w), 2970 (m), 2997 (w), 3051 (w), 3065 (w).

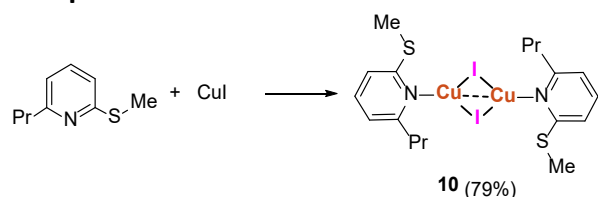
CP 9



A mixture of 6-hydroxymethyl-2-(methylsulfanyl)pyridine (83 mg, 0.53 mmol) and CuI (203 mg, 1.06 mmol) in MeCN (2 mL) was stirred until dissolution of CuI. The formed white powder of **9** was then centrifuged, washed with cold MeCN (1 x 1 mL) and dried in vacuum. Yield: 243 mg (85%). Anal. Calcd. for $C_7H_9Cu_2I_2NOS$ (536.12): C, 15.7; H, 1.7; N, 2.6. Found: C, 15.8; H, 1.7; N, 2.4. FT-IR (KBr, cm^{-1}): $\nu = 413$ (w), 499 (w), 623 (w),

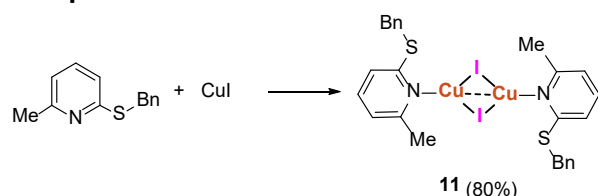
687 (w), 725 (w), 773 (s), 878 (w), 962 (m), 1009 (m), 1038 (vs), 1148 (w), 1169 (s), 1207 (w), 1252 (w), 1288 (w), 1385 (s), 1412 (s), 1421 (s), 1437 (vs), 1450 (s), 1558 (vs), 1583 (m), 2855 (w), 2924 (w), 3372 (vs).

Complex 10



A mixture of 2-(methylsulfanyl)-6-propylpyridine (111 mg, 0.66 mmol) and CuI (120 mg, 0.63 mmol) in MeCN (7 mL) was stirred until dissolution of CuI. The resulting solution was poured on a Petri dish and evaporated on air. The crystallized colorless powder of **10** was collected and dried in vacuum. Yield: 178 mg (79%). Anal. Calcd. for $C_{18}H_{26}Cu_2I_2N_2S_2$ (715.44): C, 30.2; H, 3.7; N, 3.9. Found: C, 30.0; H, 3.7; N, 3.8. FT-IR (KBr, cm^{-1}): $\nu = 440$ (w), 692 (w), 746 (w), 789 (s), 860 (w), 910 (w), 968 (w), 1009 (w), 1063 (w), 1090 (w), 1103 (w), 1180 (s), 1254 (w), 1285 (vw), 1379 (w), 1402 (m), 1437 (vs), 1449 (s), 1560 (s), 1584 (s), 2855 (w), 2868 (w), 2926 (m), 2959 (m).

Complex 11



A mixture of 2-(benzylsulfanyl)-6-methylpyridine (70 mg, 0.32 mmol) and CuI (59 mg, 0.31 mmol) in MeCN (8 mL) was stirred until dissolution of CuI. The resulting solution was poured on a Petri dish and evaporated on air. The crystallized colorless powder of **11** was collected and dried in vacuum. Yield: 100 mg (80%). Anal. Calcd. for $C_{26}H_{26}Cu_2I_2N_2S_2$ (811.5): C, 38.5; H, 3.2; N, 3.5. Found: C, 38.3; H, 3.3; N, 3.4. FT-IR (KBr, cm^{-1}): $\nu = 426$ (w), 486 (m), 579 (w), 692 (s), 706 (s), 773 (s), 866 (m), 918 (w), 991 (w), 1028 (w), 1069 (w), 1101 (w), 1157 (m), 1177 (vs), 1204 (w), 1242 (m), 1377 (m), 1435 (vs), 1450 (vs), 1495 (m), 1566 (s), 1589 (s), 2843 (vw), 2920 (w), 2951 (vw), 2980 (vw), 3032 (w), 3084 (vw).

§3. Single crystal X-ray crystallography

Single crystals of **1–11** were grown by slow evaporation of a acetonitrile solution of corresponding complex at ambient temperature for 1–3 days. Diffraction data for **1**, **2**, and **9** were collected on an automated Agilent Xcalibur diffractometer equipped with an area AtlasS2 detector (graphite monochromator, $\lambda(MoK\alpha) = 0.71073 \text{ \AA}$, ω -scans). The data for **3–8**, **10**, and **11** were collected on a Bruker Kappa Apex II CCD diffractometer using ϕ, ω -scans of narrow (0.5°) frames with $MoK\alpha$ radiation ($\lambda = 0.71073 \text{ \AA}$) and a graphite monochromator. Integration, absorption correction, and determination of unit cell parameters were performed using the CrysAlisPro program package.³ The structures were solved by dual space algorithm (SHELXT⁴) and refined by the full-matrix least squares technique (SHELXL⁵) in the anisotropic approximation (except hydrogen atoms). Positions of hydrogen atoms of organic ligands were calculated geometrically and refined in the riding model.

The crystallographic data and refinement details are summarized in Table S1. CCDC 1585190–1585192, 1585525–1585527, 1585529, 1585530, 2165799–2165802 contain the supplementary crystallographic data

for this paper. These data can be obtained free of charge from The Cambridge Crystallographic Data Center at <https://www.ccdc.cam.ac.uk/structures/>.

Table S1. Data collection and refinement parameters for **1–11**.



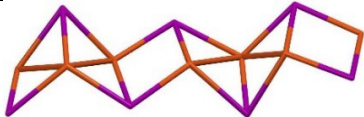
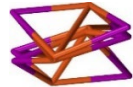
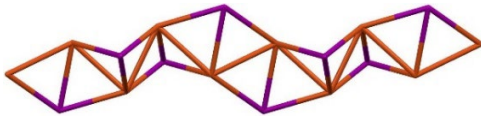
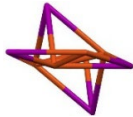
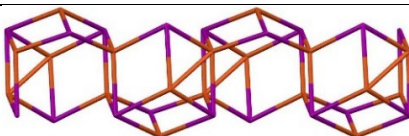




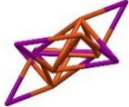

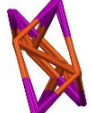
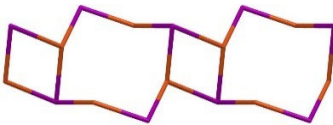
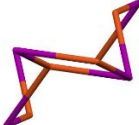
Compound	1	2	3 (296 K)	3 (125 K)	4	5
CCDC number	1585191	1585192	1585530	2165800	1585529	1585527
Empirical formula	C ₆ H ₇ CuINS	C ₆ H ₇ Cu ₂ I ₂ NS	C ₇ H ₉ Cu ₂ I ₂ NS	C ₇ H ₉ Cu ₂ I ₂ NS	C ₂₀ H ₃₀ Cu ₃ I ₃ N ₂ S ₂	C ₁₂ H ₁₁ Cu ₂ I ₂ NS
Formula mass (g/mol)	315.63	506.07	520.09	520.09	933.90	582.16
Space group	<i>P</i> −1	<i>P</i> −1	<i>P</i> −1	<i>P</i> −1	<i>P</i> 2/ <i>n</i>	<i>P</i> 2/ <i>n</i>
Temperature (K)	130	130	296	125	296	296
<i>a</i> , <i>b</i> , <i>c</i> (Å)	8.4448(2), 10.1110(2), 11.2974(3)	7.6287(6), 7.7189(3), 9.7933(7)	7.3111(4), 8.5758(5), 10.1694(6)	7.2585(3), 8.4812(4), 10.1289(4)	9.6879(5), 10.7084(6), 13.9460(7)	8.2845(3), 7.8286 (3), 24.1700(8)
α , β , γ (°)	82.916(2), 71.120(2), 67.334(2)	102.595(5), 94.694(6), 104.937(5)	77.594(2), 79.841(2), 89.519(2)	78.063(1), 79.381(1), 88.740(1)	102.975(2)	96.482(1)
<i>V</i> (Å ³)	842.24(4)	537.93(6)	612.67(6)	599.53(4)	1409.85(13)	1557.55(10)
Crystal size (mm)	0.31 × 0.18 × 0.10	0.32 × 0.24 × 0.16	0.35 × 0.25 × 0.15	0.40 × 0.20 × 0.10	0.50 × 0.20 × 0.15	0.20 × 0.10 × 0.06
<i>Z</i>	4	2	2	2	2	4
μ (mm ^{−1})	6.43	9.83	8.64	8.83	5.69	6.81
No. of measured, independent and observed [<i>I</i> > 2 σ (<i>I</i>)] reflections	13803, 4716, 4377	8550, 2670, 2438	11000, 2688, 2490	12782, 3922, 3560	30118, 4126, 3612	17220, 3558, 3231
<i>R</i> _{int}	0.021	0.028	0.039	0.048	0.045	0.051
<i>R</i> [<i>F</i> ² > 2 σ (<i>F</i> ²)], <i>wR</i> (<i>F</i> ²), <i>S</i>	0.018, 0.040, 1.10	0.022, 0.046, 1.10	0.026, 0.069, 1.09	0.025, 0.064, 1.05	0.021, 0.054, 1.06	0.036, 0.098, 1.07
No. of reflections	4716	2670	2688	3922	4126	3558
No. of parameters	183	110	121	120	137	146
$\Delta\rho_{\max}$, $\Delta\rho_{\min}$ (e Å ^{−3})	0.83, −0.50	0.71, −0.98	0.84, −0.83	0.99, −1.38	0.39, −0.64	2.40, −1.53

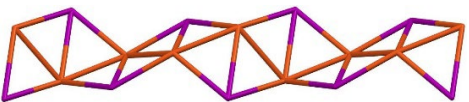
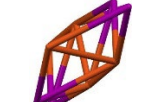


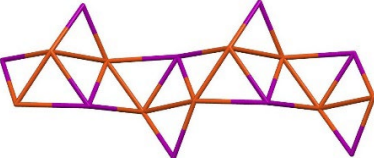

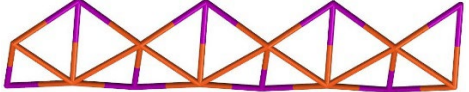

Table S1 (continued). Data collection and refinement parameters for **1–11**.

Compound	6	7	8	9	10	11
CCDC number	2165799	1585526	1585525	1585190	2165802	2165801
Empirical formula	C ₈ H ₁₁ Cu ₂ I ₂ NOS	C ₁₀ H ₁₅ Cu ₂ I ₂ NOS	C ₈ H ₁₁ Cu ₂ I ₂ NOS	C ₇ H ₉ Cu ₂ I ₂ NOS	C ₁₈ H ₂₆ Cu ₂ I ₂ N ₂ S ₂	C ₂₆ H ₂₆ Cu ₂ I ₂ N ₂ S ₂
Formula mass (g/mol)	550.12	578.17	550.12	536.09	715.41	811.49
Space group	<i>P</i> 2 ₁ / <i>c</i>	<i>P</i> 2 ₁ / <i>n</i>	<i>P</i> 2 ₁ / <i>c</i>	<i>P</i> 2 ₁ / <i>c</i>	<i>P</i> 2 ₁ / <i>n</i>	<i>P</i> 2 ₁ / <i>n</i>
Temperature (K)	296	296	296	130	296	296
<i>a</i> , <i>b</i> , <i>c</i> (Å)	10.6275(3), 16.1635(4), 8.2621(2)	13.2768(4), 7.4401(2), 15.2595(5)	4.3651(2), 19.7496(11), 15.8828(9)	9.7476(4), 9.7854(3), 13.1877(5)	10.0644(7), 8.5333(7), 14.2287(12)	11.5255(9), 10.2674(7), 12.1602(9)
α , β , γ (°)	102.226(1)	95.530(1)	95.378(3)	102.066(4)	97.604(4)	97.018(3)
<i>V</i> (Å ³)	1387.05(6)	1500.33(8)	1363.21(13)	1230.11(8)	1211.25(17)	1428.22(18)
Crystal size (mm)	0.80 × 0.25 × 0.10	0.70 × 0.40 × 0.20	0.80 × 0.20 × 0.03	0.41 × 0.34 × 0.09	0.90 × 0.20 × 0.10	0.80 × 0.80 × 0.40
<i>Z</i>	4	4	4	4	2	2

μ (mm ⁻¹)	7.64	7.07	7.78	8.61	4.48	3.81
No. of measured, independent and observed [$I > 2\sigma(I)$] reflections	15989, 3182, 2824	20729, 4074, 3766	16722, 2400, 2277	10103, 3054, 2697	21069, 3321, 2433	27893, 3976, 2879
R_{int}	0.034	0.049	0.047	0.031	0.041	0.048
$R[F^2 > 2\sigma(F^2)]$, $wR(F^2)$, S	0.023, 0.054, 1.02	0.027, 0.068, 1.07	0.057, 0.137, 1.02	0.025, 0.051, 1.04	0.044, 0.149, 1.02	0.055, 0.146, 1.02
No. of reflections	3182	4074	2400	3054	3321	3976
No. of parameters	139	157	138	131	120	155
$\Delta\rho_{\text{max}}$, $\Delta\rho_{\text{min}}$ (e Å ⁻³)	0.63, -0.91	1.38, -1.14	1.74, -2.03	0.87, -1.11	1.54, -1.35	1.94, -2.10

Table S2. Structural types of one-dimensional Cu_xl_x chains.

General view	View along 1D chain	Reference
		<i>CrystEngComm</i> , 2010 , 12, 2203.
		<i>CrystEngComm</i> , 2010 , 12, 2203.
		<i>Faraday Discuss.</i> , 2014 , 170, 93; <i>Polyhedron</i> 2018 , 151, 171; <i>J. Struct. Chem.</i> , 2019 , 60, 617; <i>J. Struct. Chem.</i> , 2020 , 61, 894; <i>Dalton Trans.</i> , 2021 , 50, 9317; CP 2 in this work
		<i>Inorg. Chem.</i> , 2021 , 60, 13528.
		<i>Dalton Trans.</i> , 2021 , 50, 9317; <i>CrystEngComm</i> , 2022 , 24, 341.
		<i>J. Mater. Chem. C</i> , 2015 , 3, 6249.
		<i>CrystEngComm</i> , 2005 , 7, 249.
		NEW TYPE CP 3 in this work

		NEW TYPE CP 5 in this work
		NEW TYPE CP 6 in this work
		NEW TYPE CP 7 in this work
		NEW TYPE CP 8 in this work

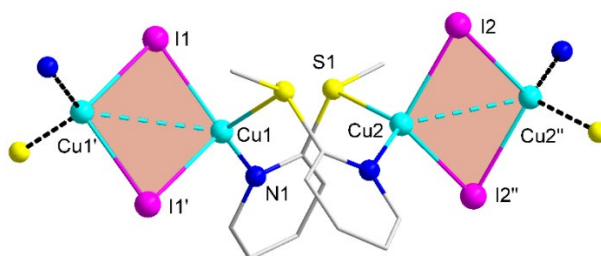


Figure S1. A fragment of 1D chain of **1** (the H atoms are omitted). Selected interatomic distances (Å): Cu1...Cu1' 3.2334(5), Cu2...Cu2'' 3.0646(4), Cu1–N1 2.0322(18), Cu2–S1 2.3693(6), Cu1–I1 2.6432(3), Cu1–I1' 2.6877(3), Cu2''–I2 2.6749(3). Symmetry codes: (') -x+1, -y, -z; (") -x, -y+1, -z+1.

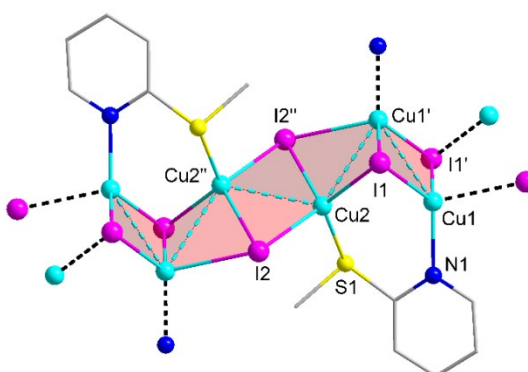


Figure S2. A fragment of 1D chain of **2** (the H atoms are omitted). Selected interatomic distances (Å): Cu1...Cu1' 2.7412(8), Cu1...Cu2 3.0456(6), Cu1'...Cu2 2.9015(6), Cu2...Cu2'' 2.8332(8), Cu1–N1 2.049(3), Cu2–S1 2.3171(9), Cu1–I1 2.6413(5), Cu1–I1' 2.6663(5), Cu1'–I1 2.6664(5), Cu2–I1 2.5935(5), Cu2–I2 2.6703(5), Cu2–I2'' 2.6894(5). Symmetry codes: (') -x+1, -y+1, -z; (") -x, -y+1, -z.

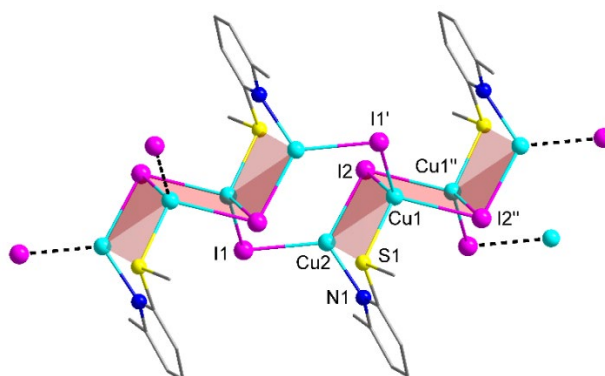


Figure S3. A fragment of 1D chain of **3** (296 K, the H atoms are omitted). Selected interatomic distances (Å): Cu1...Cu1'' 2.9519(8), Cu1...Cu2 3.0304(7), Cu1–S1 2.3630(11), Cu2–S1 2.8986(12), Cu2–N1 2.015(3), Cu1–I2 2.6276(6), Cu1–I2'' 2.7070(6), Cu1–I1' 2.6137(6), Cu1''–I2 2.7070(6), Cu2–I1 2.5265(6), Cu2–I2 2.5381(6). Symmetry codes: (') -x, -y+1, -z+1; (") -x+1, -y+1, -z+1.

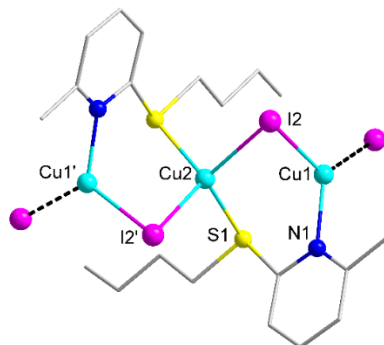


Figure S4. A fragment of 1D chain of **4** (the H atoms are omitted). Selected interatomic distances (Å): Cu1...Cu2 3.1632(3), Cu2–S1 2.3894(6), Cu1–N1 2.0168(16), Cu1–I2 2.5397(3), Cu2–I2 2.6314(3), Cu2–I2' 2.6314(3). Symmetry code: (') -x+1.5, y, -z+0.5.

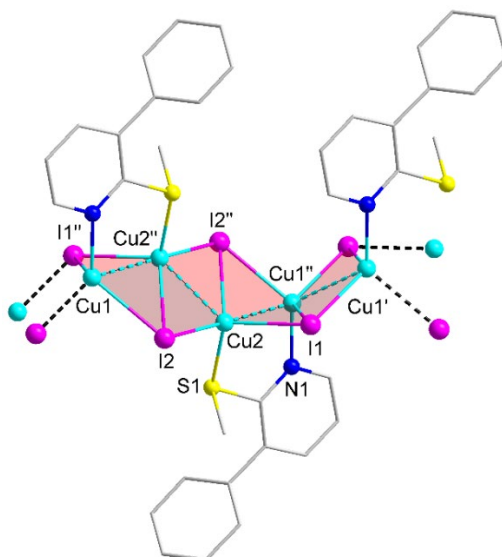


Figure S5. A fragment of 1D chain of **5** (the H atoms are omitted). Selected interatomic distances (Å): Cu1...Cu2'' 2.6101(9), Cu2...Cu2'' 2.6831(13), Cu2...Cu1'' 2.6102(9), Cu2–S1 2.3398(17), Cu1''–N1 2.059(5), Cu1'–I1 2.6327(8), Cu2–I1 2.6422(8), Cu1''–I1 2.7379(9), Cu2–I2 2.6127(7), Cu2''–I2 2.6760(8), Cu1–I2 2.7286(8). Symmetry codes: (') x-1, y, z; (") -x+1, -y, -z.

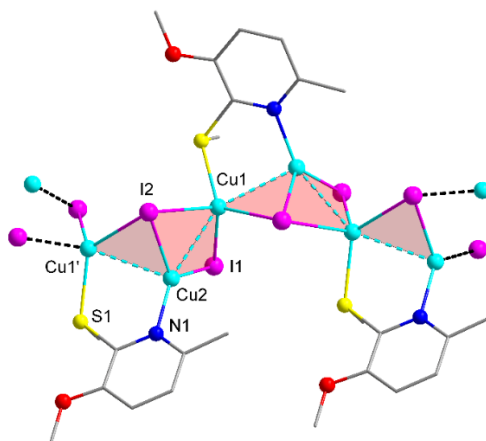


Figure S6. A fragment of 1D chain of **6** (the H atoms are omitted). Selected interatomic distances (Å): Cu1...Cu2 2.6827(6), Cu1'...Cu2 2.7534(6), Cu2–N1 2.005(3), Cu1'–S1 2.3142(10), Cu1–I1 2.6045(5), Cu1–I2 2.7617(5), Cu2–I1 2.5145(5), Cu2–I2 2.6141(5), Cu1'–I2 2.6609(5). Symmetry code: (') $x, -y+0.5, z-0.5$.

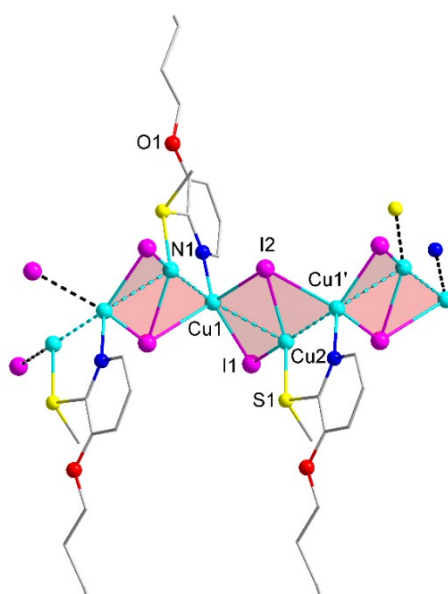


Figure S7. A fragment of 1D chain of **7** (the H atoms are omitted). Selected interatomic distances (Å): Cu1...Cu2 2.8328(7), Cu2...Cu1' 2.6285(6), Cu1–N1 2.051(3), Cu2–S1 2.2924(9), Cu1–I1 2.6164(5), Cu1–I2 2.7572(5), Cu2–I1 2.5732(5), Cu2–I2 2.5812(5), Cu1'–I2 2.7506(5). Symmetry code: (') $-x+1.5, y-0.5, -z+1.5$.

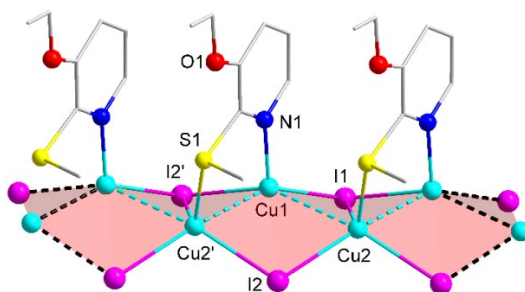


Figure S8. A fragment of 1D chain of **8** (the H atoms are omitted). Selected interatomic distances (Å): Cu1...Cu2 2.787(3), Cu1...Cu2' 2.577(3), Cu1–N1 2.060(11), S1–Cu2' 2.336(4), Cu1–I1 2.5999(19), Cu1–I2 2.948(2), Cu2–I1 2.708(2), Cu2'–I2 2.677(2). Symmetry code: (') $x+1, y, z$.

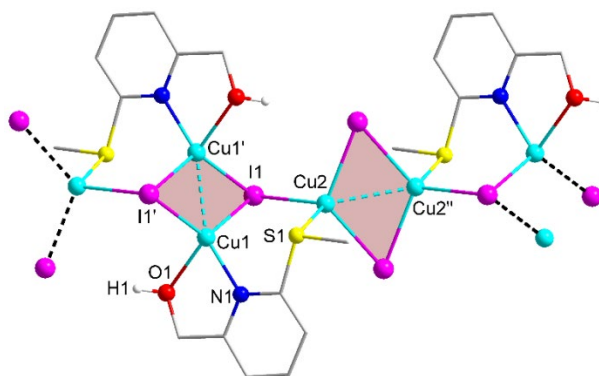


Figure S9. A fragment of 1D chain of **9** (the H atoms are omitted). Selected interatomic distances (Å): Cu1...Cu1' 2.4812(9), Cu2...Cu2'' 2.6375(8), Cu1–O1 2.220(3), Cu1–N1 2.009(3), Cu2–S1 2.3583(10), Cu1–I1 2.6389(5), Cu1–I1' 2.5758(5), Cu2–I1 2.6256(5), Cu2–I2 2.6159(5), O1–H1 0.854(19). Symmetry codes: (') $-x+1, -y+1, -z+1$; (") $-x, -y+1, -z+1$.

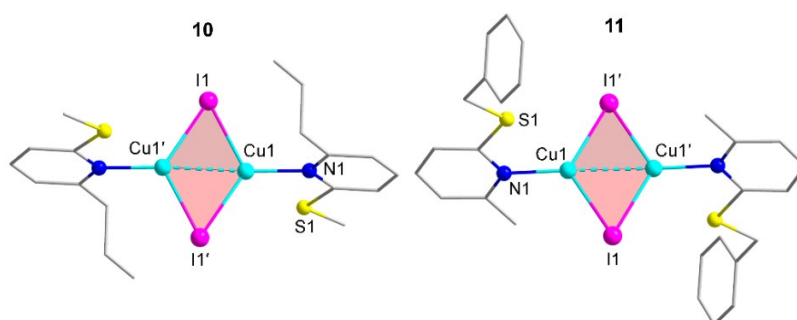
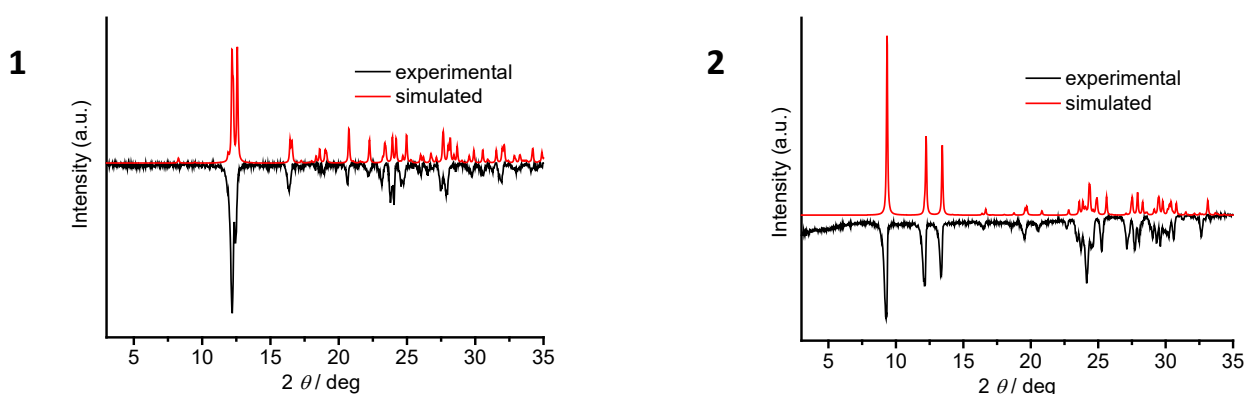


Figure S10. Structures of **10** and **11** (the H atoms are omitted). Selected interatomic distances in **10** (Å): Cu1...Cu1' 2.6074(11), Cu1–N1 2.007(3), Cu1–S1 3.0060(18), Cu1–I1 2.5760(7). Symmetry code: (') $-x+1, -y, -z$. Selected interatomic distances in **11** (Å): Cu1...Cu1' 2.6680(15), Cu1–N1 2.009(5), Cu1–I1 2.5721(9), Cu1–S1 3.0670(19). Symmetry code: (') $-x, -y+1, -z+2$.

§4. Powder X-ray diffraction patterns



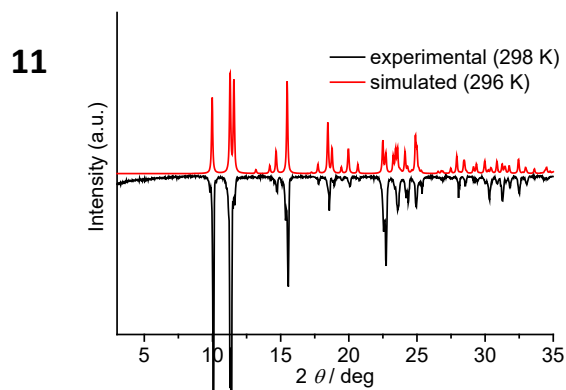
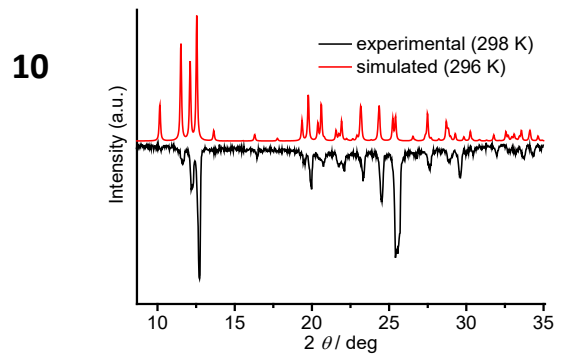
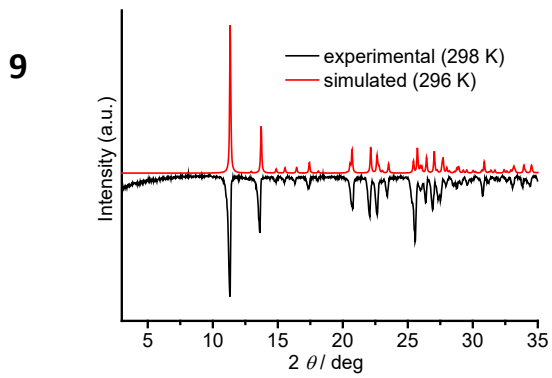
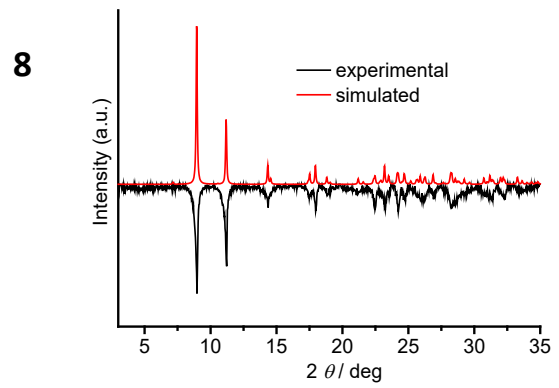
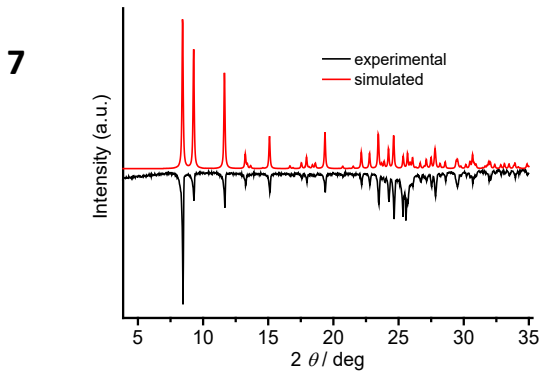
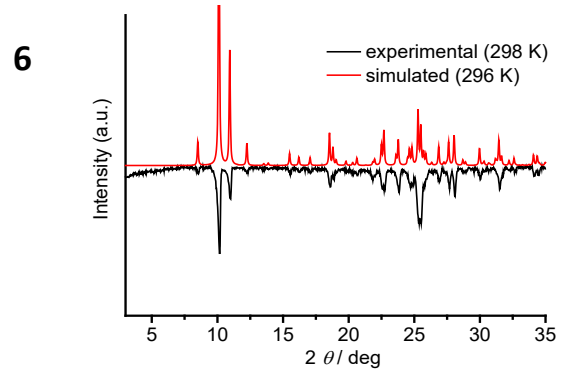
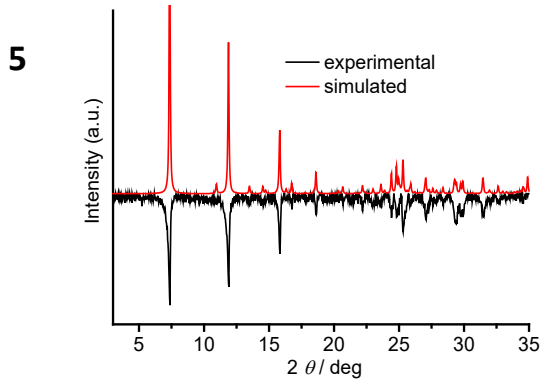
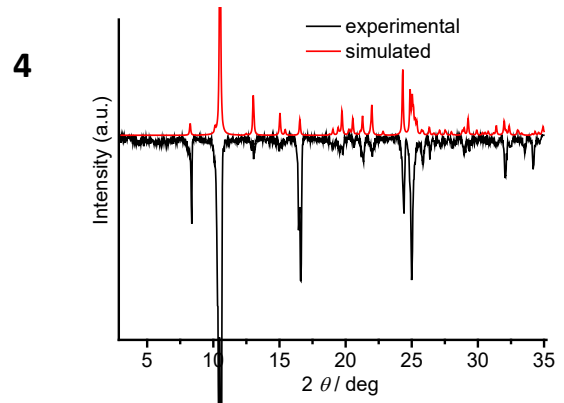
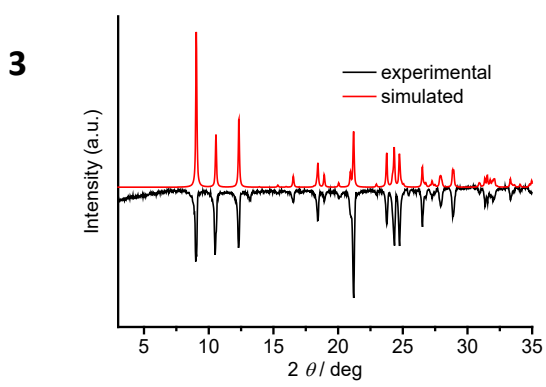


Figure S11. Experimental and simulated PXRD patterns for **1–11**.

§5. TGA curves

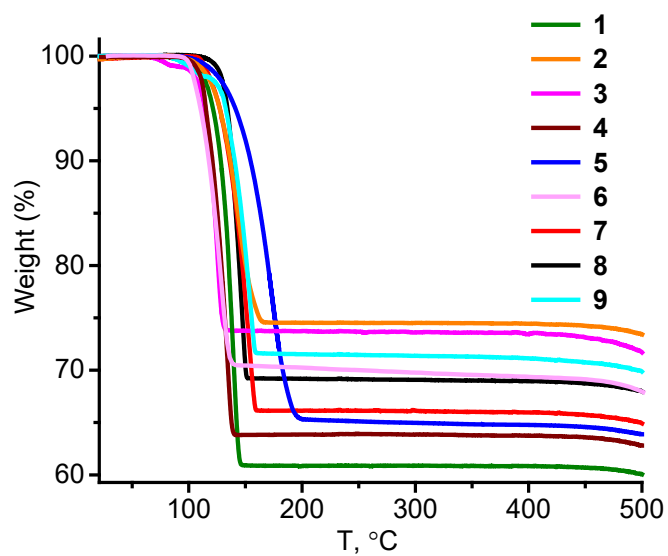


Figure S12. TGA curves for CPs **1–9**.

Table S3. Experimental and calculated weight losses associated with thermal elimination of the ligands from CPs **1–9**.

Weight loss, %	1	2	3	4	5	6	7	8	9
Calculated	38.7	24.7	26.8	38.8	34.6	29.6	34.1	30.8	28.9
Experimental	39.1	25.3	26.2	36.2	34.7	30.7	33.8	30.7	28.2

§6. FT-IR spectra

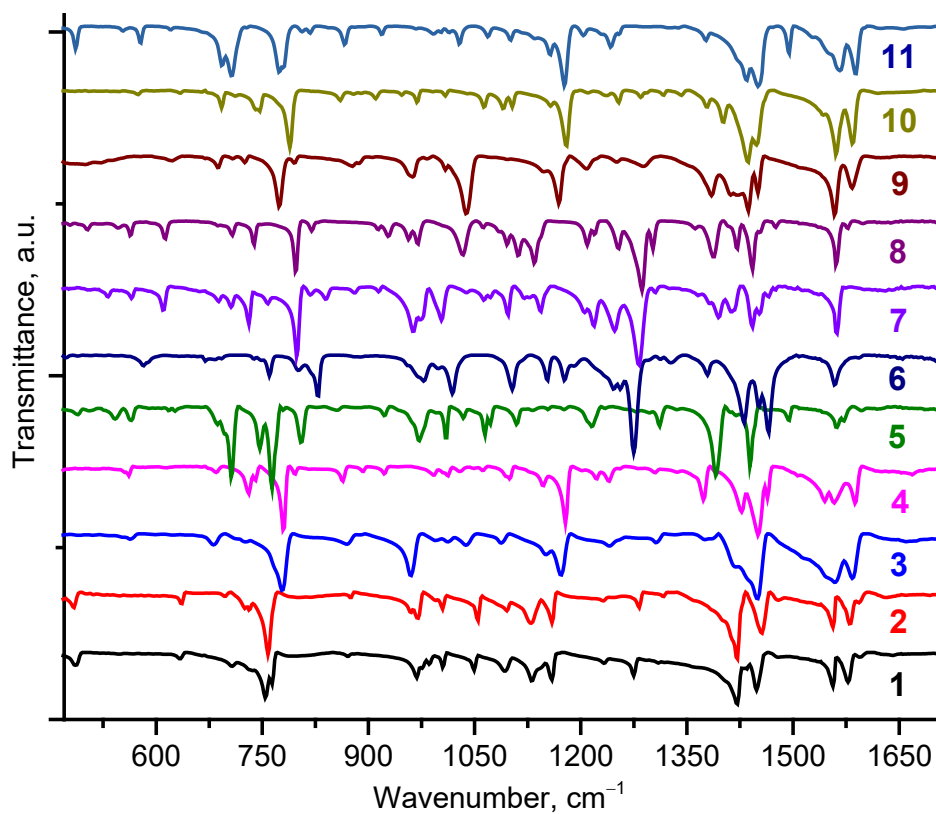


Figure S13. FT-IR spectra of **1–11** viewed in the fingerprint area.

§7.1. Electronic structure calculations

The density of states (DOS) of selected compounds were calculated employing the Cambridge Serial Total Energy Package (CASTEP)⁶ using the crystal structures obtained from single crystal X-Ray diffraction analysis without modifications. Generalized gradient approximation (GGA) with Perdew-Burke-Ernzerhof (PBE) exchange correlation functional (xc) were used for all calculations. Ultrasoft pseudopotentials were used for all chemical elements and the total energy tolerance was set to be 1×10^{-5} eV/atom. The plane-wave kinetic energy cut-off is 351 eV.

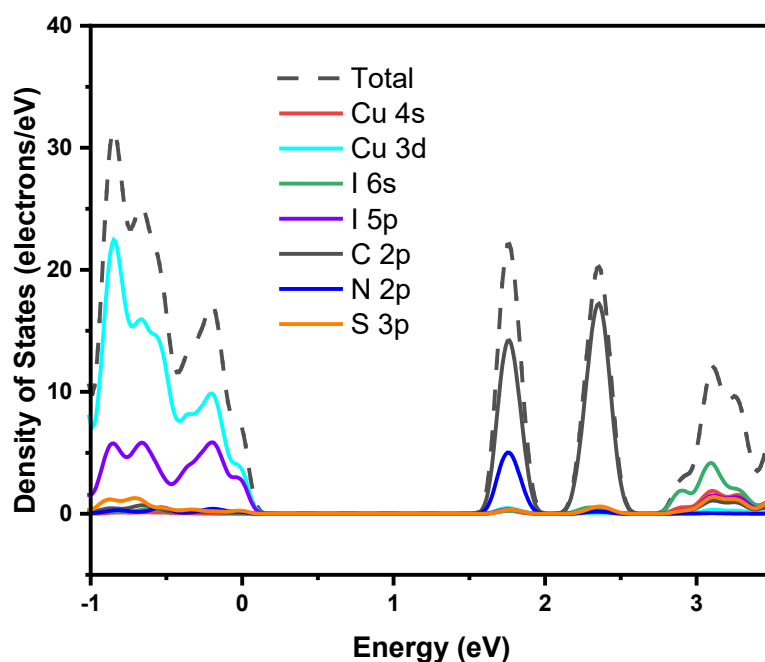


Figure S14. Calculated projected density of states of CP 2.

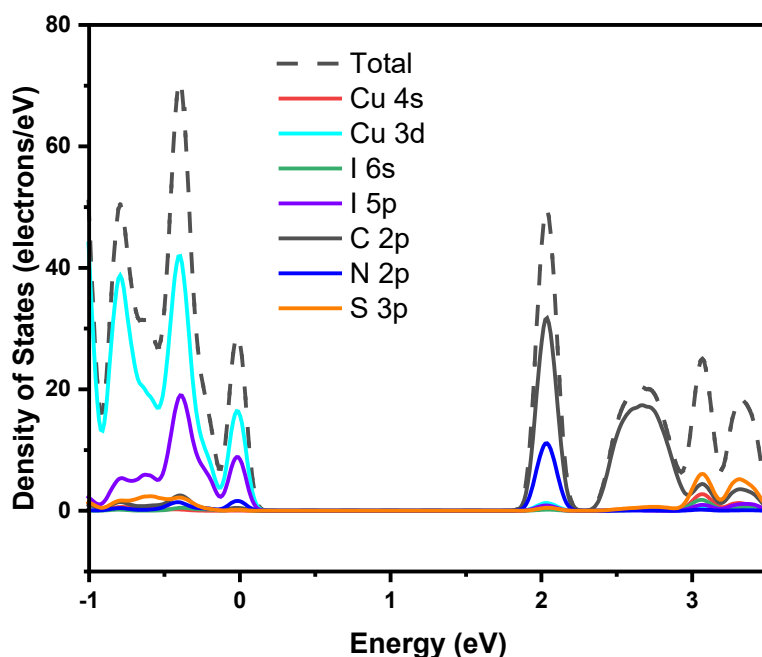


Figure S15. Calculated projected density of states of CP **4**.

§7.2. QTAIM and ELF calculations

Computation details. The QTAIM and ELF calculations based on the experimental X-ray geometries of **1–11** have been carried out in Gaussian-09 suite⁷ using the dispersion-corrected hybrid functional ω B97XD.⁸ The Douglas–Kroll–Hess 2nd order scalar relativistic calculations requested relativistic core Hamiltonian were carried out using the DZP-DKH basis sets^{9–12} for all atoms. The topological analysis of the electron density distribution has been performed by using the Multiwfn program (version 3.7).¹³

Discussion

Hereafter, we have assessed metallophilic interactions in compounds **1–3** and **5–11**, in which the Cu⋯Cu contacts (*vide supra*) are shorter than the twice van der Waal radius of Cu (2.80 Å).¹⁴ To this end, X-ray derived model fragments of **1–11** were computed at the DFT level of theory. Except for **1**, **3** (at 296 K) and **4**, all the compounds studied reveal the presence of bond critical points (3, -1) (BCP), indicating the Cu⋯Cu interactions. As an example, the calculated Cu⋯Cu bonding in **9** is illustrated in Figure S16. The parameters of the BCPs in **2**, **3** (at 125 K) and **5–11** (Table S4) are typical for the metal⋯metal interactions. The listed data indicate noticeable covalent contribution in the Cu⋯Cu interactions [$-G(\mathbf{r})/V(\mathbf{r}) < 1$],¹⁵ and their attractive nature ($\lambda_2 < 0$).¹⁶

Table S4. Values of the density of all electrons – $\rho(\mathbf{r})$, Laplacian of electron density – $\nabla^2\rho(\mathbf{r})$ and appropriate λ_2 eigenvalues, energy density – H_b , potential energy density – $V(\mathbf{r})$, Lagrangian kinetic energy – $G(\mathbf{r})$, and electron localization function – ELF (a.u.) at the bond critical points (3, -1) (BCP), corresponding to the Cu⋯Cu interactions in of **1–11**.

$d_{\text{Cu}\cdots\text{Cu}}$, Å	$\rho(\mathbf{r})$	$\nabla^2\rho(\mathbf{r})$	$-\lambda_2$	$-H_b$	$-V(\mathbf{r})$	$G(\mathbf{r})$	ELF
			1				
3.065				BCP was not found			

3.233				BCP was not found				
4.049				BCP was not found				
2								
2.741	0.027	0.028	0.027	0.008	0.024	0.015	0.172	
2.833	0.022	0.031	0.022	0.005	0.019	0.013	0.129	
2.902				BCP was not found				
3.046				BCP was not found				
3 (at 125 K)								
2.834	0.022	0.032	0.022	0.005	0.019	0.013	0.129	
3.049				BCP was not found				
3.955				BCP was not found				
4.094				BCP was not found				
3 (at 296 K)								
2.952				BCP was not found				
3.030				BCP was not found				
3.927				BCP was not found				
4.133				BCP was not found				
4								
3.613				BCP was not found				
5								
2.610	0.034	0.028	0.034	0.013	0.033	0.020	0.202	
2.682	0.029	0.028	0.029	0.010	0.027	0.017	0.172	
2.683	0.029	0.029	0.029	0.010	0.027	0.017	0.181	
6								
2.683				BCP was not found				
2.753	0.026	0.031	0.026	0.008	0.024	0.016	0.140	
7								
2.628	0.033	0.025	0.033	0.013	0.032	0.019	0.202	
2.833				BCP was not found				
8								
2.577	0.035	0.028	0.035	0.014	0.036	0.021	0.209	
2.787	0.024	0.032	0.024	0.007	0.022	0.015	0.136	
9								
2.481	0.043	0.033	0.043	0.018	0.044	0.026	0.259	
2.638	0.032	0.028	0.032	0.012	0.031	0.019	0.196	
3.585				BCP was not found				
10								
2.607	0.037	0.022	0.037	0.014	0.033	0.019	0.263	
11								
2.668	0.033	0.025	0.033	0.011	0.029	0.018	0.234	

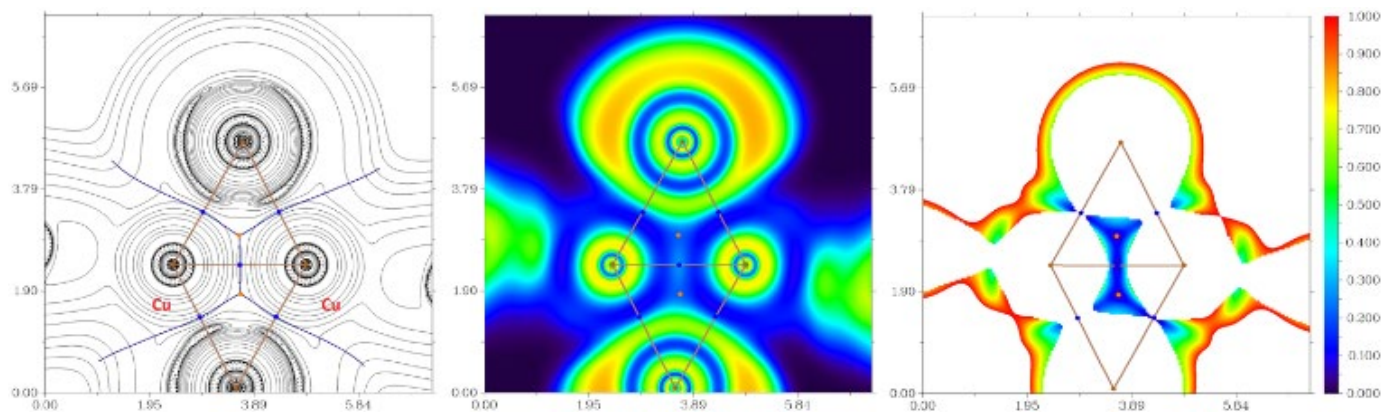


Figure 16. Metallophilic interactions in CP **9**. *Left panel:* contour line diagram of the Laplacian of electron density distribution $\nabla^2\rho(\mathbf{r})$, bond paths, and selected zero-flux surfaces; *Center panel:* visualization of electron localization function; *Right panel:* reduced density gradient analyses. Bond critical points (3, -1) are shown in blue, nuclear critical points (3, -3) – in pale brown, ring critical points (3, +1) – in orange, bond paths are shown as pale brown lines, length units – Å, and the color scale for the ELF and RDG maps is presented in a.u.

§8. Photophysical data

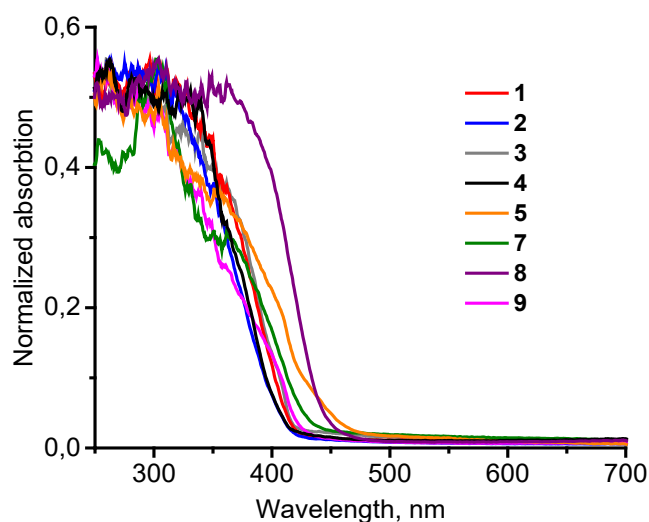


Figure S17. Normalized UV-Vis absorption spectra (plotted as Kubelka-Munk functions) of solid CPs **1–9** (298 K).

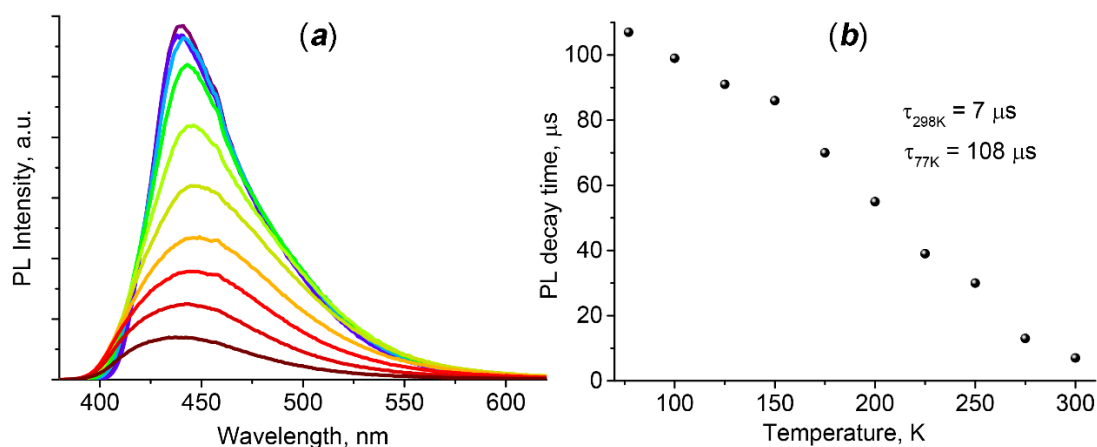


Figure S18. (a) Temperature dependent emission spectra of **4** ($\lambda_{\text{ex}} = 370 \text{ nm}$); (b) PL decay times of **4** against temperature ($\lambda_{\text{ex}} = 350 \text{ nm}$, $\lambda_{\text{em}} = 450 \text{ nm}$).

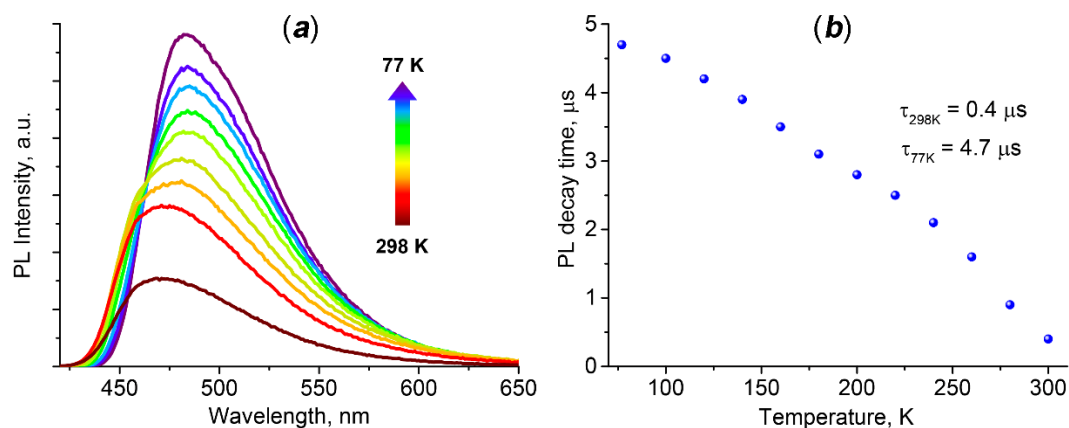


Figure S19. (a) Temperature dependent emission spectra of **8** ($\lambda_{\text{ex}} = 400 \text{ nm}$); (b) PL decay times of **8** against temperature ($\lambda_{\text{ex}} = 400 \text{ nm}$, $\lambda_{\text{em}} = 480 \text{ nm}$).

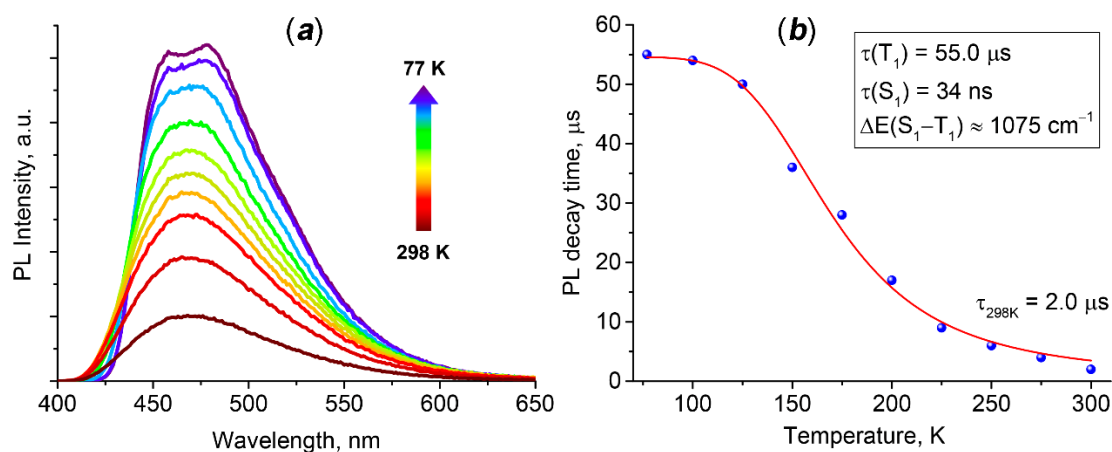


Figure S20. (a) Temperature dependent emission spectra of **9** ($\lambda_{\text{ex}} = 360 \text{ nm}$); (b) PL decay times of **9** against temperature ($\lambda_{\text{ex}} = 350 \text{ nm}$, $\lambda_{\text{em}} = 470 \text{ nm}$). The fitting curve is derived from the equation 1 (see main text).

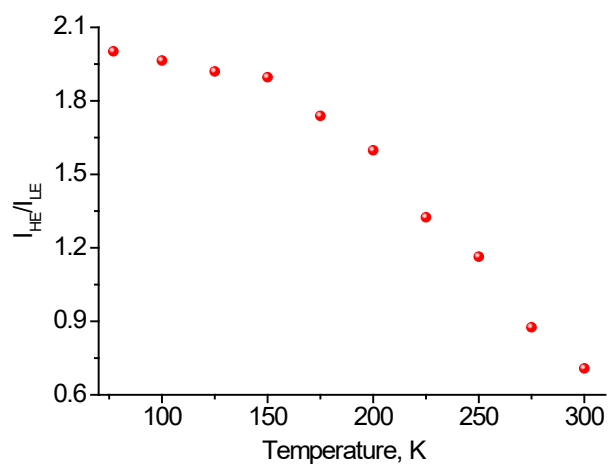


Figure S21. Intensity integral ratio of the HE and LE bands of **3** against temperatures ($\lambda_{ex} = 420$ nm).

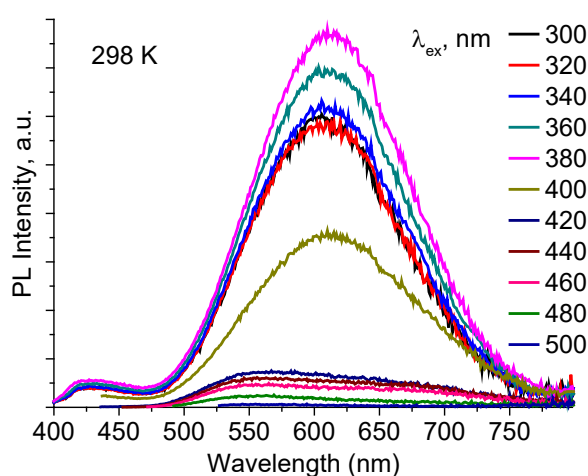
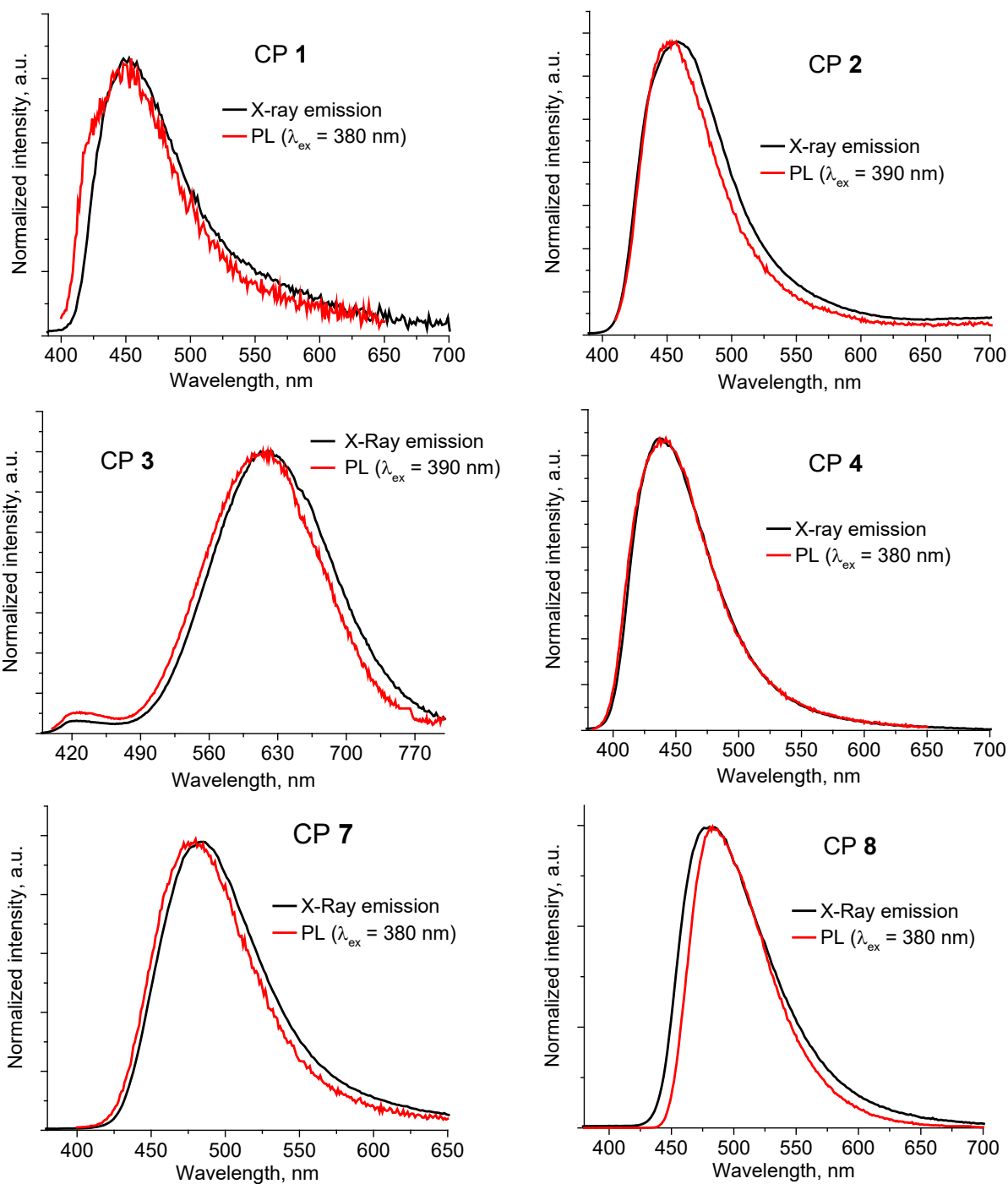


Figure S22. Excitation dependent PL spectra of **3** at 298 K.

§9. X-Ray radioluminescence

X-ray radioluminescence (RL) spectra were recorded on a home-built spectrometer¹⁷ following the earlier developed protocol for powder samples;¹⁸ further technical details on possible experimental artifacts and spectral processing can be found in ref.¹⁹ The sample of neat solid in the form of an island of finely ground powder with dimensions 3 x 8 mm and thickness of about 0.1 mm, applied via a stencil on a vertical aluminum plate with polypropylene-based double-sided Scotch tape, was directly exposed to the incident X-ray beam (unfiltered bremsstrahlung from a CW X-ray tube 2,5BSV-27-Mo, Svetlana, St. Petersburg, Russia, 40 kV x 20 mA, sample distance to anode 210 mm) and to the light-collecting optics of the detection system comprising a quartz optical imaging system, a grating monochromator (MDR-206, LOMO Photonics, St Petersburg, Russia, objective focus length 180 mm, grating 1200 lines per mm, inverse linear dispersion 4.3 nm mm⁻¹) with slits set to 2.2 mm/2.2 mm (spectral resolution about 10 nm), and a Hamamatsu H10493-012 photosensor module. All experiments were performed at ambient conditions in air without environmental control. To assess compound stability under irradiation, four consecutive spectra (512 wavelength points in the range 250 to 1000 nm) of single wavelength scans of 18 min each were recorded from freshly prepared samples, the gradual sagging of spectra is indicative of the degradation rate of unprotected neat powder under irradiation in air. The RL spectra given in the main text are averages of the four spectra. All RL spectra

were recorded in nominally identical conditions and were normalized to sample amount in moles, the y-axes, although given in “arbitrary units”, can be directly compared between different spectra. For quantification of luminous efficiency of the samples studied, RL of a reference sample of bismuth germanate (BGO) was also recorded using the same procedure (spectra given in Fig. S30 below, normalized using $\text{Bi}_4\text{Ge}_4\text{O}_{12}$ as “molecular unit”). In the RL spectra, the emission line was integrated up to line maximum to produce AUC values, and the ratio of AUC value for the sample to AUC value for BGO was taken as the measure of luminous efficiency χ_E (Table S6).¹⁸



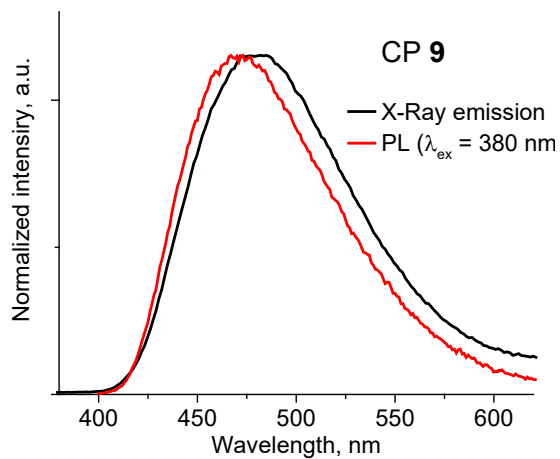
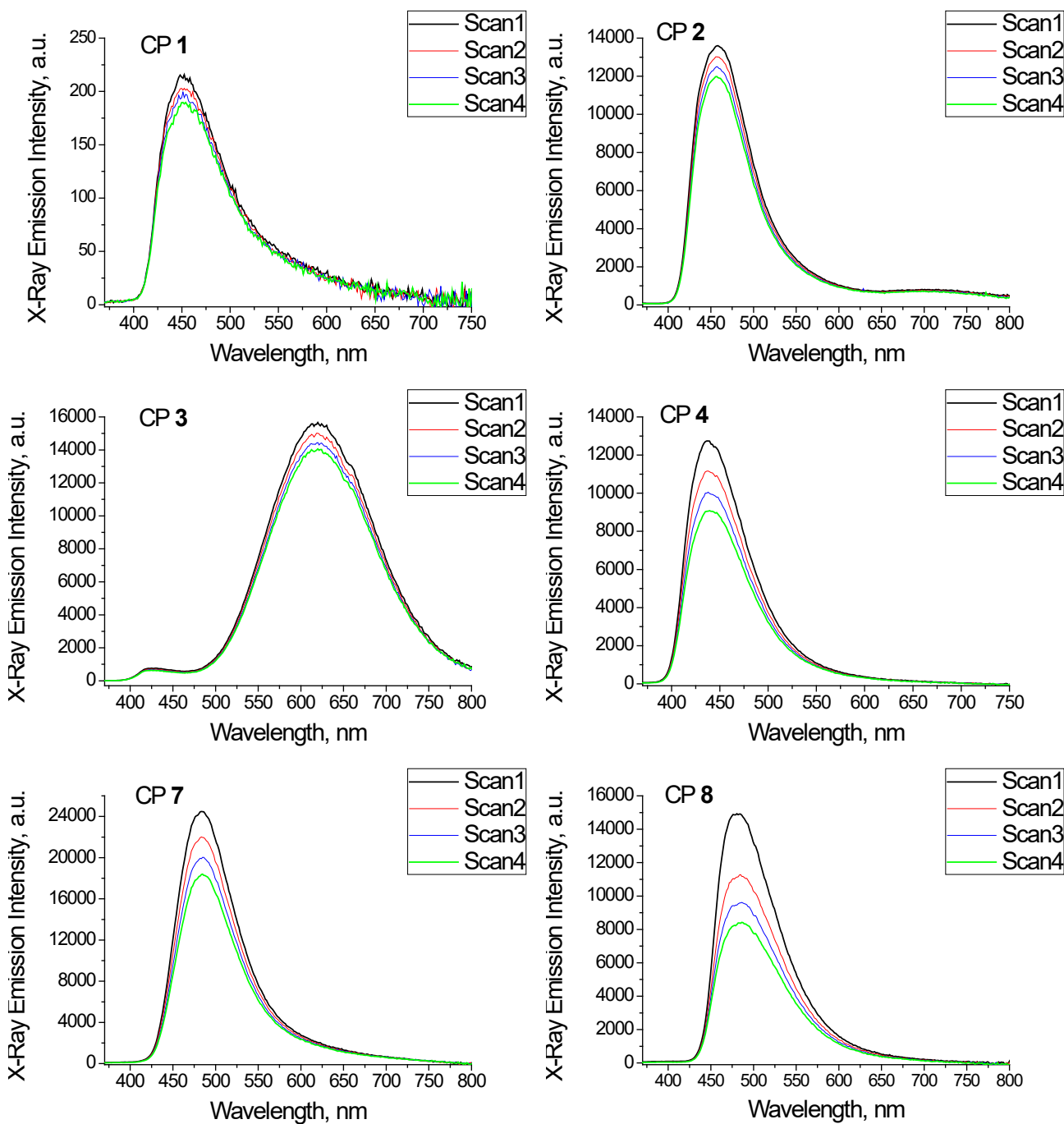


Figure S23. Comparison of PL and RL spectra of CPs 1–4 and 7–9.



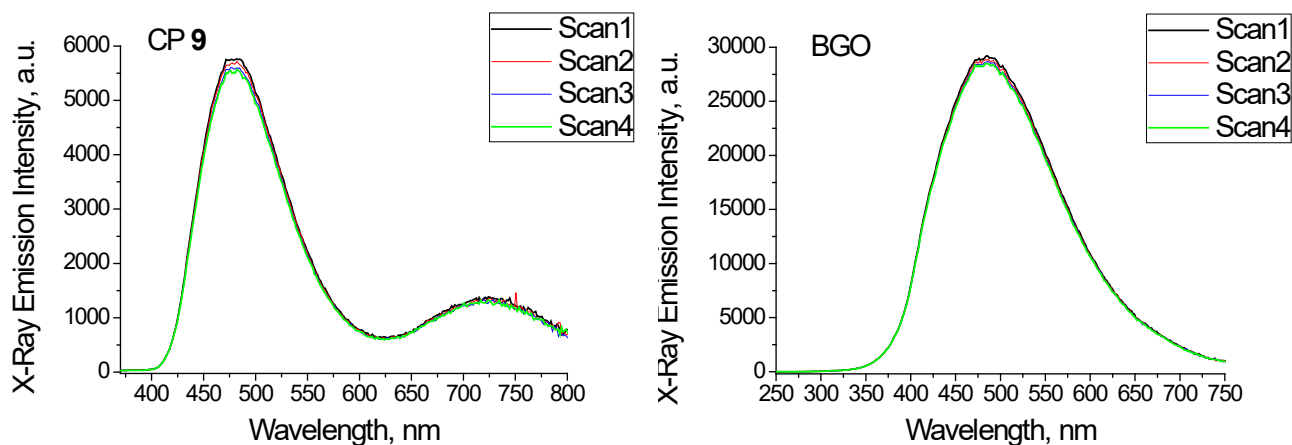


Figure S24. Comparison of X-ray stability of CPs 1–4 and 7–9, as well as BGO (reference).

Table S5. RL efficiency of 1–4 and 7–9 relative to BGO (reference).

CP	λ_{\max} , nm	AUC, a.u.	$X_E = \text{AUC}/\text{AUC}_{\text{BGO}}$
1	452	6.1×10^3	0.0031
2	457	3.9×10^5	0.20
3	618	1.1×10^6	0.55
4	440	3.1×10^5	0.16
7	484	7.4×10^5	0.37
8	485	3.6×10^5	0.18
9	479	2.2×10^5	0.11
BGO	485	2.0×10^6	1.0

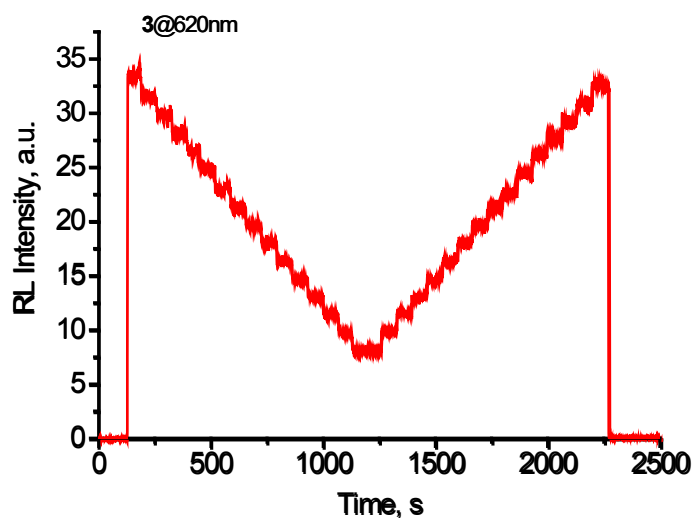


Figure S25. Check of linearity of RL response vs. dose rate for CP 3. Detection wavelength was set at emission maximum, and emission intensity as raw signal from detector was recorded while varying anode current of the X-ray tube from nominal (20 mA) down to 5mA and back to 20 mA in 1 mA steps, recording signal for 1 min at each step (2 min at 5 mA). The accelerating voltage was held constant (40 kV), and thus anode current was directly proportional to dose rate, so the produced graph gives the dependence of emission intensity on dose rate over 4:1 range, clearly demonstrating a linear dose rate response. Upon returning back to nominal anode current the signal does not return exactly to the initial level due to sample degradation, as shown in Fig. S31 above.

§10. References

- 1 O.A. Tarasova, N.A. Nedolya, A.I. Albanov, B.A. Trofimov, *Russ. J. Org. Chem.*, **2017**, *53*, 130–133.
- 2 N.A. Nedolya, O.A. Tarasova, A.I. Albanov, B.A. Trofimov, *Russ. J. Org. Chem.*, **2017**, *53*, 134–136.
- 3 CrysAlisPro, Rigaku Oxford Diffraction, 2015. Version: 1.171.38.46.
- 4 G.M. Sheldrick, *Acta Cryst. A*, **2015**, *71*, 3–8.
- 5 G.M. Sheldrick, *Acta Cryst. C*, **2015**, *71*, 3–8.
- 6 S.J. Clark, M.D. Segall, C.J. Pickard, P.J. Hasnip, M.I.J. Probert, K. Refson, M.C. Payne, *Z. für Krist. - Cryst. Mater.*, **2005**, *220*, 567–570.
- 7 M.J. Frisch et al. Gaussian 09, Revision C.01, Gaussian Inc., Wallingford, CT, 2010.
- 8 J.-D. Chaia, M. Head-Gordon, *Phys. Chem. Chem. Phys.*, **2008**, *10*, 6615–6620.
- 9 C.L. Barros, P.J.P. de Oliveira, F.E. Jorge, A. Canal Neto, M. Campos, *Mol. Phys.*, **2010**, *108*, 1965–1972.
- 10 F.E. Jorge, A. Canal Neto, G.G. Camiletti, S.F. Machado, *J. Chem. Phys.*, **2009**, *130*, 064108.
- 11 A. Canal Neto, F.E. Jorge, *Chem. Phys. Lett.*, **2013**, *582*, 158–162.
- 12 R.C. de Berrêdo, F.E. Jorge, *J. Mol. Struct. Theochem*, **2010**, *961*, 107–112.
- 13 T. Lu, F. Chen, *J. Comput. Chem.*, **2012**, *33*, 580–592.
- 14 A. Bondi, van der Waals Volumes and Radii, *J. Phys. Chem.*, **1964**, *68*, 441–451.
- 15 E. Espinosa, I. Alkaorta, J. Elguero and E. Molins, *J. Chem. Phys.*, **2002**, *117*, 5529–5542.
- 16 E. R. Johnson, S. Keinan, P. Mori-Sánchez, J. Contreras García, A. J. Cohen and W. Yang, *J. Am. Chem. Soc.*, **2010**, *132*, 6498–6506.
- 17 E.V. Kalneus, A.R. Melnikov, V.V. Korolev, V.I. Ivannikov, D.V. Stass, *Appl. Magn. Reson.*, **2013**, *44*, 81–96.
- 18 D.V. Evtushok, A.R. Melnikov, N.A. Vorotnikova, Y.A. Vorotnikov, A.A. Ryadun, N.V. Kuratieva, K.V. Kozyr, N.R. Obedinskaya, E.I. Kretov, I.N. Novozhilov, Y.V. Mironov, D.V. Stass, O.A. Efremova, M.A. Shestopalov, *Dalton Trans.*, **2017**, *46*, 11738–11747.
- 19 D.V. Stass, N.A. Vorotnikova, M.A. Shestopalov, *J. Appl. Phys.*, **2021**, *129*, 183102.